Dual resonance approach to decoupling surface and bulk attributes in photonic crystal biosensor

Md Nazmul Hossain,* John Justice, Pierre Lovera, Alan O'Riordan, and Brian Corbett

Tyndall National Institute, University College Cork, Lee Maltings, Cork, Ireland
**Corresponding author: nazmul.hossain@tyndall.ie*

Received September 12, 2014; revised October 3, 2014; accepted October 5, 2014;
posted October 6, 2014 (Doc. ID 223017); published October 23, 2014

A sub-wavelength grating-based photonic crystal sensor is designed to excite two spectrally and spatially different guided mode resonances that have distinctive electric field distributions. We present and validate the uni-polarized dual resonance approach to separating bulk index perturbations from surface-binding events in a single measurement by monitoring the resonance wavelength shifts. This self-referencing method will reduce errors in the measurement of biomolecule binding events on sensor surfaces in a perturbed environmental background. © 2014 Optical Society of America

OCIS codes: (280.4788) Optical sensing and sensors; (050.5298) Photonic crystals; (280.1415) Biological sensing and sensors; (050.6624) Subwavelength structures.
http://dx.doi.org/10.1364/OL.39.006213

Label-free optical sensing based on the guided mode resonance (GMR) property [1–3] in photonic crystal (PhC) platforms has been used for more than a decade to detect the in-situ binding kinetics of enzymes, viruses, and cells [4,5]. Such sensors have refractive index (RI) discrimination down to 10^{-6} refractive index units (RIU) with a large dynamic range [4]. This sensing technique has been incorporated recently in a handheld smartphone-based label-free portable sensing platform [6]. Although GMR sensors are widely used for affinity sensing, the information obtained by the present mono-polarized single resonance technique is limited [7].

The resonance wavelength value (RWV) of the sensor is readily tuned by a change in the optical density of the medium lying within the range of the evanescent electric (E) field. Therefore, in addition to RI changes associated with the surface-bound target biomolecular material, thermal induced RI changes of the bulk liquid medium covering the sensor will also induce a shift in the RWV. This could be a significant problem in portable diagnostic applications where thermal variations are likely. A PhC sensor with an enhanced surface-to-bulk sensitivity [8] has been reported to suppress the noise coming from the bulk solution. But, a single resonance of polarized light, normally used for detection, cannot simultaneously resolve changes in the biolayer and the surrounding in one measurement. Magnusson *et al.* [7] have proposed a dual (TE and TM) polarization-based approach to determine individual attributes of the bulk and surface changes and avoid a separate reference site for monitoring of the background index. Though further improvement of their backfit model was suggested [7] for precise separation of the attributes of the biolayer and its surroundings, fundamentally, the spatial electric field distribution of the TE and TM resonant modes are not distinctive enough for accurate decoupling of these contributions.

In this Letter, we present a dual resonance-based discrimination method that monitors the response of two spatially (electric field) and spectrally different resonance modes to decouple the interfering surface and bulk attributes. One resonance acts as a bulk sensor because of its larger electric field penetration depth into the bulk solution, whereas the other resonance serves mostly as a surface sensor. This approach also avoids the need of a separate reference site for background monitoring. In a controlled experimental test of the dual-mode operation, we differentiate the thickness of a deposited thin layer (imitates as a biolayer) on the sensor surface, with a superimposed bulk RI variation as a perturbation.

A GMR sensor is a sub-wavelength grating structure in a single or multilayer waveguide film designed to create a narrow resonant reflection peak at a selected wavelength of certain polarization. When the light is incident normally upon a sub-wavelength grating, the zeroth order of the diffracted light is sustained while the higher order diffracted light is evanescent.

When the diffracted light from the grating structure is coupled with a leaky waveguide mode satisfying the phase-matching condition, sharp resonance peak/dips are observed at particular wavelengths in the reflection and transmission spectra [1]. Incident light at the resonance wavelength becomes spatially confined, which generates a high optical field at the sensor surface. This localized electric field extends evanescently a short distance into the test sample. This leads to a strong interaction between the structure and adsorbed biomaterial and to the ability to perform high resolution sensing of protein and cell attachment.

The GMR sensor used for our experiment consists of a partially etched sub-wavelength grating structure in a thin layer of silicon nitride (Si_3N_4) deposited on a quartz substrate as shown in Fig. 1. Λ denotes the period of the grating, h_{etch} the etching depth, and h_{wav} the thickness of the Si_3N_4 waveguide layer. The grating parameters are chosen such that only ± 1 diffraction order can exist by total internal reflection in the waveguide layer [9]. For a 55% filling fraction grating with $\Lambda = 420$ nm and $h_{wav} = 450$ nm, h_{etch} is varied to investigate its role in the resonance spectra.

Figure 2 shows mapping of the transmission spectra of the sensor for different etching depths carried out using a finite-difference time-domain (FDTD) simulator [10]. For shallow etching (up to 250 nm), the sensor sustains two

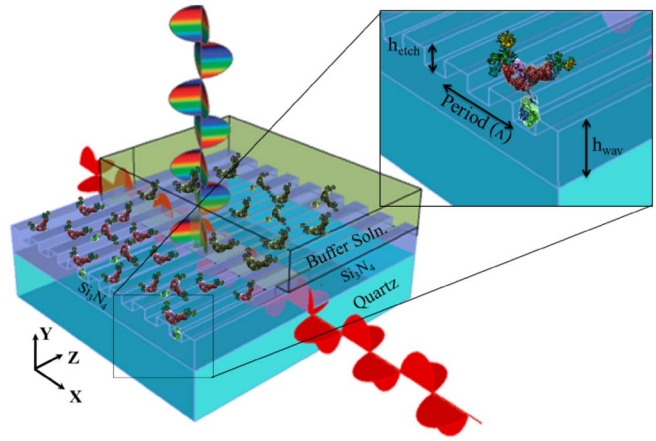

Fig. 1. Schematic of the PhC biosensor where Λ = period of the grating, h_{etch} = etching depth, $h_{\text{wav}} = Si_3N_4$ waveguide layer thickness. The buffer solution on top contains the bioanalytes. (The antibody–antigen complexes shown in the schematic are not at the same scale as the grating.)

resonances, whereas for deep etching (depth greater than 250 nm), the 1st resonance fades out while the 2nd resonance is sustained. As the etching depth increases, the effective index of the Si_3N_4 waveguide layer reduces, and so the resonance wavelength shifts to lower wavelength. The full width at half-maximum (FWHM) of the resonance peaks also change with etching depth.

A doubly resonant [11] 1D PhC GMR sensor with an etching depth of 190 nm is studied further. Figure 3 shows the distinctive E-field distribution of the two resonance modes when illuminated by a mono-polarized (E-field parallel to the grating lines) broadband planewave light source. The resonances are found at wavelengths of 619 and 736 nm, which are distinctive by their spectral shape (FWHM) (Fig. 2 inset) and electric field distribution (Fig. 3). The 1st resonance (at 619 nm) acts as a bulk sensor because of its higher E-field penetration depth into the bulk solution, whereas the 2nd resonance (at 736 nm) serves mostly as a surface sensor.

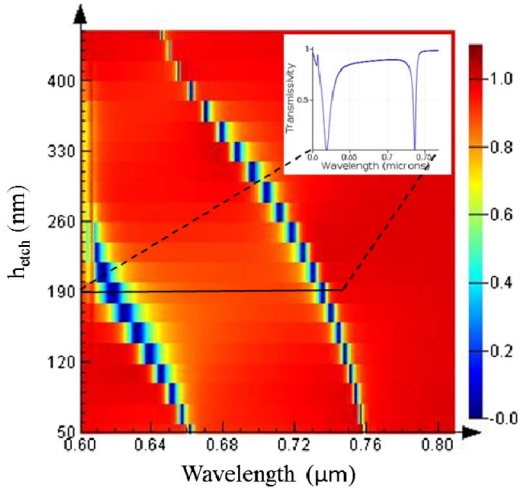

Fig. 2. Transmission spectra map showing the resonance wavelengths (blue colored regions shows resonance dips) for different etch depths. Inset shows the transmission spectrum for an etching depth of 190 nm.

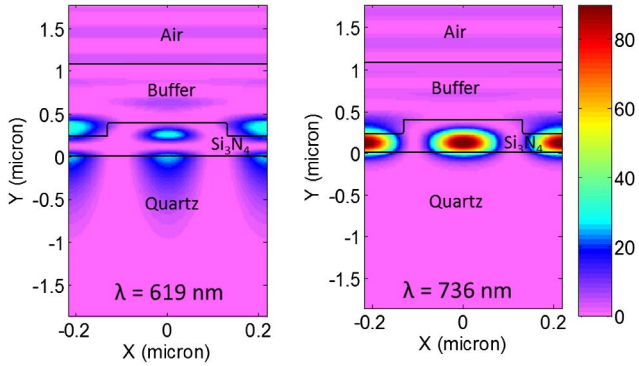

Fig. 3. FDTD modeled E-field distribution of PhC unit cell with an etching depth of 190 nm resonating at wavelengths, λ, of 619 and 736 nm.

The shift in the resonance wavelength occurs because of RI changes of the bulk liquid medium and the formation of thin layer of biomolecules on the sensor surface. The functional dependence of the measured wavelength shift ($\Delta\lambda$) of each resonance as the result of both the change in added layer thickness (Δd) and bulk index (Δn) is expressed as

$$\begin{pmatrix} \Delta\lambda_1 \\ \Delta\lambda_2 \end{pmatrix} = \begin{pmatrix} \frac{\partial\lambda_1}{\partial d} & \frac{\partial\lambda_1}{\partial n} \\ \frac{\partial\lambda_2}{\partial d} & \frac{\partial\lambda_2}{\partial n} \end{pmatrix} \times \begin{pmatrix} \Delta d \\ \Delta n \end{pmatrix}. \quad (1)$$

The subscripts 1 and 2 in Eq. (1) denote the 1st and 2nd resonance, respectively. The respective differential values of the matrix in Eq. (1) can be obtained by linearly changing the added layer thickness and RI of bulk solution. This can be done either from the FDTD simulations shown in Figs. 4(a) and 4(b) or from experimental measurements. Based on these differential values and the shift of each resonance peak found from the experiment, the added layer thickness and the bulk index change can be calculated from a single experiment using Eq. (1).

The PhC is patterned by electron beam lithography, and then the pattern is transferred into the Si_3N_4 layer by a nanofabrication technique [12] where Chrome is used as the hard mask. To validate the dual-mode operation in biosensing, we differentiate the thickness of the attached thin layer on sensor surface, with superimposed bulk RI variation as a perturbation.

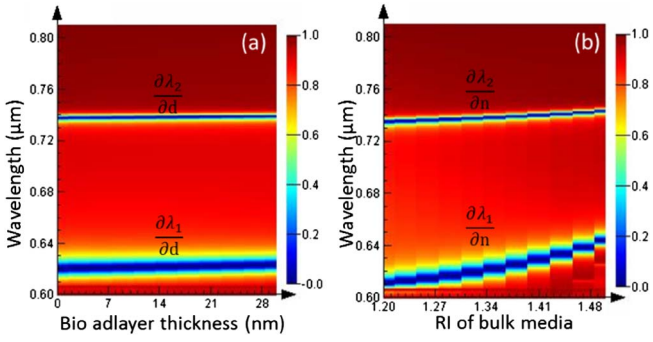

Fig. 4. Map of the transmission spectrum of the PhC sensor for (a) different added layer thickness, Δd and (b) RI of bulk medium, n.

The transmission spectrum of the sensor with DI water on top (Fig. 5) shows two resonances at the wavelength of 618.6 and 739.4 nm. The experimentally found 1st RWV matches with the model, but the 2nd RWV is few nm longer than that of the simulated (Fig. 3) value. The FWHM of the 1st resonance (Fig. 5) is also broader than that calculated (Fig. 2) unlike the 2nd resonance. This can be associated with the sidewall roughness of the grating lines and the spatial position of E-field of each resonance.

A 16-nm-thin layer of silicon dioxide (SiO_2) of RI 1.45 comparable to the RI of biomolecules is coated on the sensor surface. The transmission spectrum of the thin layer-coated sensor is measured again with different bulk solution to imitate the scenario of a bulk index perturbation during biomolecular attachment. The bulk solution on top of the sensor is changed from DI water (RI = 1.332) to isopropyl-alcohol (RI = 1.3776). The change in both bulk index and surface layer together yield a total RWV shift of 10.4 and 1.9 nm for the 1st and 2nd resonance, respectively.

Sensors based on single resonance cannot distinguish between the individual contributions from surface and bulk. But, the two-resonance approach provides separate values of additional layer (Δd) and index change (Δn) by monitoring the RWV shift of both resonances. The respective differential values (listed below) of the matrix in Eq. (1) have been obtained from a separate experiment on the fabricated sensor where the RI of the bulk solution and the added layer thickness are linearly changed individually (RI: 1.33 → 1.38 and Δd:0 → 16 nm) and the change in resonance wavelengths are measured.

$$\frac{\partial\lambda_1}{\partial d} = 0.04375; \qquad \frac{\partial\lambda_1}{\partial n} = 205.7 \text{ nm/RIU},$$
$$\frac{\partial\lambda_2}{\partial d} = 0.05; \qquad \frac{\partial\lambda_2}{\partial n} = 21.9 \text{ nm/RIU}.$$

Here, the sensitivity of the 1st resonance to the surrounding bulk index, $(\partial\lambda_1/\partial n)$, is 10 times higher than that of the 2nd resonance $(\partial\lambda_2/\partial n)$. This is due to the distinctive nature of the E-field distribution of the 1st resonance, which has higher penetration depth into the bulk solution compared to the 2nd resonance.

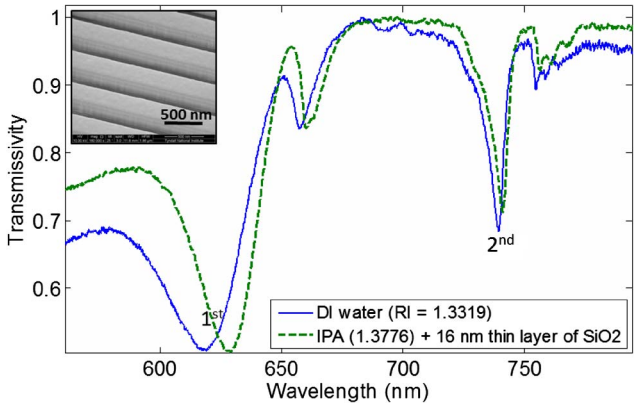

Fig. 5. Resonance wavelengths shift when the bulk solution is changed from DI water to IPA along with a thin added layer (16 nm) on the sensor surface. Inset shows the SEM image of the sensor grating.

Table 1. Sensitivity Comparison of Two Different Approaches to Bulk Index

Dual Resonance Approach		Polarization-Based Approach	
1st resonance	205.7 nm/RIU	TM resonance	54.7 nm/RIU
2nd resonance	21.9 nm/RIU	TE resonance	21.9 nm/RIU
1st: 2nd = 9.4		TM:TE = 2.5	

Using the measured resonance shift of $\Delta\lambda_1 = 10.4$ nm and $\Delta\lambda_2 = 1.9$ nm (Fig. 5), Eq. (1) gives the added layer thickness and bulk RI change as

$$\begin{pmatrix} \Delta d \\ \Delta n \end{pmatrix} = \begin{pmatrix} 17.5 \text{ nm} \\ 0.0467 \end{pmatrix}.$$

The dual-resonance approach thus could follow the change in both bulk and surface properties taking into consideration the amount of shift in the 1st and 2nd resonances and their interdependency. The proposed method calculates the added layer thickness as 17.5 nm and bulk RI change as 0.0467, which are very near to the engineered perturbation values of 16 nm and 0.0457.

In order to compare the dual-resonance scheme with the polarization-based approach presented in [7], the bulk (surrounding index) sensitivity for TM and TE polarization are measured. This is done for 2nd resonance because this sharp resonance with particular E-field distribution is typically used for GMR-based biosensing. As shown in Table 1, the dual resonance approach gives sensitivity ratio of 9.4, whereas the polarization based approach can offer 2.5. The higher contrast in the bulk sensitivity for the dual-resonance approach helps decouple the attributes of the biolayer and its surroundings leading to increased detection accuracy and reduced probability of false readings in bioassay experiments.

In summary, the proposed sensor sustains two resonance modes with their E-field distribution being distinctive in a way that one acts as a bulk sensor, whereas the other behaves primarily as a surface sensor. Taking benefit of the different behavior of the two coexisting resonances, a new approach to separating bulk and surface properties is proposed and validated. It leads to a self-referenced biosensor robust against environmental background noise. Furthermore, multiple resonances in combination with different polarizations with resulting diverse E-field distributions of interest could lead to a better understanding of the biomolecular interaction. This multi-parametric approach to biosensing will assist in revealing additional information in proteomics and clinical diagnostic applications instead of just quantifying the analytes.

This research has been carried out with the support of Science Foundation Ireland under the Irish Photonic Integration Centre (IPIC) award 12/RC/2276 and EU FP7-ICT PHAST-ID project under grant agreement 258238.

References

1. S. S. Wang and R. Magnusson, Appl. Opt. **32**, 2606 (1993).

2. Y. Ding and R. Magnusson, Opt. Express **12**, 5661 (2004).
3. A. Ricciardi, S. Campopiano, A. Cusano, T. F. Krauss, and L. O'Faolain, IEEE Photon. J. **2**, 696 (2010).
4. B. Cunningham, B. Lin, J. Qiu, P. Li, J. Pepper, and B. Hugh, Sens. Actuator B **85**, 219 (2002).
5. Y. Fang, A. M. Ferrie, and G. S. Li, FEBS Lett. **579**, 4175 (2005).
6. D. Gallegos, K. D. Long, H. J. Yu, P. P. Clark, Y. X. Lin, S. George, P. Nath, and B. T. Cunningham, Lab Chip **13**, 2124 (2013).
7. R. Magnusson, D. Wawro, S. Zimmerman, and Y. Ding, Sensors **11**, 1476 (2011).
8. N. Ganesh, I. D. Block, and B. T. Cunningham, Appl. Phys. Lett. **89**, 023901 (2006).
9. R. Magnusson, Opt. Lett. **37**, 3792 (2012).
10. Lumerical Solutions, Inc., http://www.lumerical.com/tcad-products/fdtd/.
11. M. N. Hossain, J. Justice, P. Lovera, M. Mitchell, A. Oriordan, and B. Corbett, in *Frontiers in Optics*, OSA Technical Digest (online) (Optical Society of America, 2013), paper FM4E.5.
12. M. N. Hossain, J. Justice, P. Lovera, B. McCarthy, A. O'Riordan, and B. Corbett, Nanotechnology **25**, 355301 (2014).